Homogenization and free-vibration analysis of elastic metamaterial plates by Carrera Unified Formulation finite elements

Homogenization and free-vibration analysis of elastic metamaterial plates by CUF finite elements

M. Cinefra[1], A.G. de Miguel[1], M. Filippi[1], C. Houriet[2], A. Pagani[1], E. Carrera[1]

(1) Department of Aeronautics and Space Engineering, Politecnico di Torino, Italy
(2) Unité de Mécanique, ENSTA Paristech, France

Keywords:
Free-Vibration, Finite Element Method, Homogenization, Carrera's Unified Formulation, passive periodic structure.

Author and address for Correspondence
Dr. Maria Cinefra
Associate Professor,
Department of Mechanical and Aerospace Engineering
Politecnico di Torino,
Corso Duca degli Abruzzi, 24,
10129 Torino, ITALY,
tel +39.011.546.6845, fax +39.011.564.6899
e.mail: maria.cinefra@polito.it

Abstract

This work focuses on the assessment of a novel so-called "homogenization method" allowing to transform a heterogeneous material with inclusions or holes into an equivalent homogeneous material with equal mechanical behavior. The aim is to avoid meshing holes of the real material in finite-element codes, thus improving computation time for further analysis of the material. Typical periodic structure of passive acoustic metamaterial plates is here considered, with inclusions/holes that should improve the acoustic performances in the low-frequency range. The 3D homogenization method, based on Carrera Unified Formulation [20] and Mechanics of Structure Genome, is assessed for a perforated plate made of a linear elastic material with periodic arrangement of holes. Different configurations of the metamaterial plate are considered, changing the number of the holes. The results obtained from the free-vibration analysis of the homogenized plates, performed by higher-order 2D models contained in Carrera Unified Formulation, are compared with ABAQUS results and both numerical and experimental results provided in literature.

1 Introduction

In the last decade, a new research field has emerged to study Metamaterials [1]. This term refers to materials whose properties are "beyond" those of conventional materials. They are made from assemblies of multiple elements fashioned from composite materials such as metals, foams or plastics. The core concept of metamaterial is to replace the molecules with man-made structures called unit cell. They can be viewed as "artificial atoms", usually arranged in repeating patterns on a scale much less than the relevant wavelength of the phenomena they influence. Metamaterials derive their properties not from the properties of the materials they are composed of, but from their newly designed structures with repeating patterns, hence the need for homogenization. Indeed, if it is possible to treat them like homogeneous materials with outstanding properties, their analysis becomes faster and more convenient as few adaptation to existing codes and softwares are required.
Several types of metamaterials can be found: Electromagnetic metamaterials [2, 3, 4, 5], Mechanical metamaterials [6, 7, 8]. Some are artificial three-dimensional structures which, despite being a solid, ideally behave like a fluid. Thus, they have a finite bulk modulus but vanishing shear modulus, ie. they are hard to compress yet easy to deform. And finally, Acoustic metamaterials [9, 10, 11], whose effective properties like compressibility or density can be negative. Negative density or compressibility can only be achieved dynamically. For instance, Helmholz Resonators driven just above their frequency of resonance lead to negative dynamic compressibility [12].

According to the same principles of wave propagation in periodic structures [13, 14, 15], acoustic metamaterials are tuned to the acoustic wavelength and consist of a periodic arrangement of inclusions or cylindrical pores embedded within a material matrix, that are typically spaced less than a wavelength apart. These materials disrupt the propagation of waves by scattering and refraction effects. In Acoustics, low frequencies are especially difficult to absorb with conventional materials, as the order of magnitude of the wavelength is 1 m, which is much greater than the reasonable thickness of damping materials [16]. Acoustic metamaterial are able to perform better than conventional materials because their structure is such that they do not respect physical properties like positive density or bulk modulus on a global scale at resonance - although they obviously respect physical laws at any time locally.

Finite Element Method (FEM) is well-established and yields accurate results for the structural analysis of any geometrical shape. However, it requires a mesh of all the details of the constituent material. Therefore, when dealing with plates having great numbers of holes or inclusions - such as

metamaterials, this method becomes very costly in calculations and time, especially when the macroscopic dimensions of the plate need to be much greater than the characteristic size of the holes. Thus, some homogenization methods have been investigated on the last two decades [17, 18]. In particular, Langlet et al. [19] have studied homogenization of passive periodic materials such as a plate periodically perforated across its thickness as seen in Figure 1a.

In this work, a homogenization method based on the Carrera Unified Formulation (CUF) [20] and Mechanics of Structure Genome (MSG) [21] is investigated. CUF is used to solve the governing equations of MSG for periodically heterogeneous materials. The MSG provides a tool to obtain the complete effective stiffness matrix in a straightforward manner without relying on ad-hoc assumptions and minimizing the loss of information between the original heterogeneous cell and the equivalent homogeneous body. This CUF-MSG based homogenization method has successfully been used to find the homogenized mechanical properties of composites [22], in which the unit cell, ie. the building block of the composite, is a cube containing the fiber and the matrix surrounding it. In the present article, the method is tested for another type of material: a plate with doubly periodic array of cylindrical holes. Once the effective 3D mechanical properties of the metamaterial are obtained, free-vibration analysis of the homogeneous effective material is performed by means of higher-order 2D models contained in CUF [23], to obtain its modal frequencies. The results from the CUF-MSG-based method are compared to numerical and experimental results provided by Langlet et al. [19].

2 Preliminary notions

In this paper, the linear analysis of elastic anisotropic materials will be performed. Therefore, it is mandatory to recall some preliminary notions regarding the description of the 3D strain and stress fields of the structure before presenting the models used.

2.1 Geometrical relations

According to Carrera Unified Formulation, the stresses and strains are conveniently split into in-plane and normal components, which are denoted by the subscripts p and n, respectively. The strains can be related to the displacement field $\boldsymbol{u} = \{u, v, w\}$ via the linear geometric relations:

$$\boldsymbol{\epsilon}_p = \boldsymbol{D}_p \, \boldsymbol{u} \qquad \boldsymbol{\epsilon}_n = (\boldsymbol{D}_{np} + \boldsymbol{D}_{nz})\boldsymbol{u} \tag{1}$$

wherein the differential operator arrays are defined as follows:

$$\boldsymbol{D}_p = \begin{bmatrix} \partial_x & 0 & 0 \\ 0 & \partial_y & 0 \\ \partial_y & \partial_x & 0 \end{bmatrix} \quad \boldsymbol{D}_{np} = \begin{bmatrix} 0 & 0 & \partial_x \\ 0 & 0 & \partial_y \\ 0 & 0 & 0 \end{bmatrix} \quad \boldsymbol{D}_{nz} = \begin{bmatrix} \partial_z & 0 & 0 \\ 0 & \partial_z & 0 \\ 0 & 0 & \partial_z \end{bmatrix} \tag{2}$$

with $\boldsymbol{\epsilon}_p = (\epsilon_{xx}, \epsilon_{yy}, \epsilon_{xy})$ and $\boldsymbol{\epsilon}_n = (\epsilon_{xz}, \epsilon_{yz}, \epsilon_{zz})$ and $\partial_x, \partial_y, \partial_z$ are the partial derivatives with respect to x, y, z, respectively.

2.2 Constitutive equations

The second step towards the governing equations is the definition of the 3D constitutive equations that permit the stresses to be expressed by means of the strains. The generalized Hooke's law is considered, by employing a linear constitutive model for infinitesimal deformations.

Therefore, the stress-strain relations are:

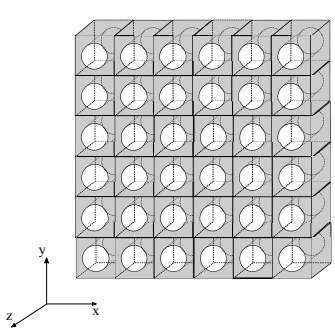

(a) Perforated Plate of PVC

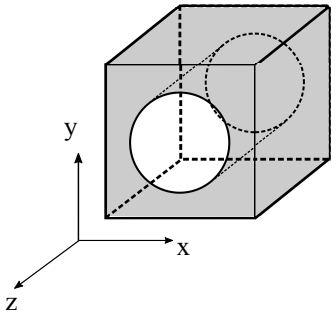

(b) Periodic Unit Cell: cube of PVC with a cylindrical void through the thickness

Figure 1: PVC material investigated. For 2D unit cell, the unit cell in the z-direction is assumed to be infinite

$$\begin{aligned} \boldsymbol{\sigma}_p &= \{\sigma_{xx}, \sigma_{yy}, \sigma_{xy}\} = \boldsymbol{C}_{pp}\, \boldsymbol{\epsilon}_p + \boldsymbol{C}_{pn}\, \boldsymbol{\epsilon}_n \\ \boldsymbol{\sigma}_n &= \{\sigma_{xz}, \sigma_{yz}, \sigma_{zz}\} = \boldsymbol{C}_{np}\, \boldsymbol{\epsilon}_p + \boldsymbol{C}_{nn}\, \boldsymbol{\epsilon}_n \end{aligned} \tag{3}$$

where

$$\begin{aligned} \boldsymbol{C}_{pp} &= \begin{bmatrix} c_{11} & c_{12} & c_{16} \\ c_{12} & c_{22} & c_{26} \\ c_{16} & c_{26} & c_{66} \end{bmatrix} \qquad \boldsymbol{C}_{pn} = \begin{bmatrix} 0 & 0 & c_{13} \\ 0 & 0 & c_{23} \\ 0 & 0 & c_{36} \end{bmatrix} \\ \boldsymbol{C}_{np} &= \begin{bmatrix} 0 & 0 & 0 \\ 0 & 0 & 0 \\ c_{13} & c_{23} & c_{36} \end{bmatrix} \qquad \boldsymbol{C}_{nn} = \begin{bmatrix} c_{55} & c_{45} & 0 \\ c_{45} & c_{44} & 0 \\ 0 & 0 & c_{33} \end{bmatrix} \end{aligned} \tag{4}$$

The material coefficients c_{ij} depend on the Young's moduli E_1, E_2, E_3, the shear moduli G_{12}, G_{13}, G_{23} and Poisson moduli ν_{12}, ν_{13}, ν_{23}, ν_{21}, ν_{31}, ν_{32} that characterize the material of the layer. Note that $(1, 2, 3)$ is the reference system of the material, in this case coincident with the global reference system (x, y, z).

3 Homogenization method

In this work, a perforated plate of PVC is investigated (Figure 1a). This plate can be divided into unit cells, smallest building blocks of the structure, each unit cell containing one cylindrical pore and a small part of the surrounding material as shown in Figure 1b.
The pores of the unit cell are chosen as cylindrical and set parallel to the z-axis as shown in Figure 1b. In Section 5, the pores are infinite in the z-dimension. Therefore the problem is bidimensional and only depends on the x and y coordinates. In Section 6, a thickness is given to the pores. In both cases, the same methods are compared: the method of Langlet et al. [19] explained in 3.1 and the CUF-MSG based method [22] is explained in details in 4.

3.1 Description of the homogenization method by Langlet et al.

In Langlet et al.[19], the material is excited by a plane, monochromatic wave characterized by a real wave vector $\boldsymbol{k}$, the modulus of which is denoted k, wave number. The natural frequency of the incident wave is ω. The boundary conditions around the unit cell verify Bloch relations.
In order to obtain the mechanical properties of the homogenized plate, the following steps are taken:

- Finite element modeling of the 2D Unit Cell for incident waves with various wave vectors k, in order to find the eigenvalues $\omega(k)$.
- A dispersion curve $\omega = f(k)$ is plotted. At low frequencies, its lowest two slopes correspond to the transversal and longitudinal velocities c_T and c_L, which are function of the porosity P and the incident angle θ.
- The plate with cylindrical holes is considered as an homogeneous anisotropic medium, with an effective density $\tilde{\rho}$ which depends on the porosity P :

$$\tilde{\rho} = (1 - P)\rho \tag{5}$$

  The Christoffel's equations are able to link $c_T(\theta)$ and $c_L(\theta)$ for any angle of incidence θ, to the effective stiffness coefficients of the effective stiffness tensor $\tilde{c}$ of the homogenized material - which are independant from θ:

$$\tilde{c} = \begin{bmatrix} \tilde{c_{11}} & \tilde{c_{12}} & 0 \\ \tilde{c_{12}} & \tilde{c_{11}} & 0 \\ 0 & 0 & \tilde{c_{66}} \end{bmatrix} \tag{6}$$

  The Christoffel's equations are particularly simple for two wave incident angles, $\theta = 0°$ and $\theta = 45°$. Thus, the finite element method yielding the transversal and longitudinal velocities needs to be used only for these two incident angles. Christoffel's equations then give the effective stiffness coefficients for the homogenized material.
- This process is repeated for various porosities in order to plot the effective stiffness constants as a function of porosity. Results are shown in Figure 3 in dotted lines. WebPlotDigitizer has been used to extract the data from the curves of Ref [19] for means of comparison.

4 A novel homogenization method based on CUF and MSG

Classical theories like First-Order Shear Deformation Theory (FSDT) based on the plate theories developed by Reissner [24] and Mindlin [25] account for shear deformation effects but are not precise enough to predict higher order shear effects. On the other hand, 3D solid finite elements methods are very common to simulate complex materials like composites, but their computational cost is often too high to be used for accurate analysis of the laminated structures.

The method investigated is based on a novel higher-order component-wise beam theory in the framework of the Carrera Unified Formulation (CUF) and yields good results for composites with few calculations [22]. To overcome the limitations of classical models and to deal with complex phenomena, such as torsion, warping, or in-plane deformation, the displacement fields of beam theory are enriched with an arbitrary number of higher-order terms [26].

4.1 Mechanics of Structure Genome

The main feature of the method investigated which leads to think it could be used to study acoustic metamaterials is the fact that it recalls the concept of the *repeating unit cell* (hereinafter RUC), just like other homogenization methods for metamaterials (Parallel Transfer Matrix Method, [27]). Moreover it is fast and simple to use, as it is able to homogenize the material only by knowing the unit cell geometry and the material properties of its components.

These capabilities are enabled by the use of the Mechanics of Structure Genome (MSG), developed by Yu et al. [21] as a unified theory for the study of multiscale structural problems. MSG is a

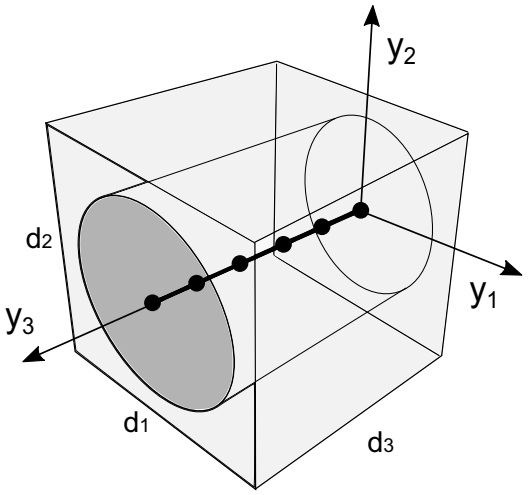

Figure 2: Reference system for the beam modeling of the RUC.

highly efficient tool to obtain the complete effective stiffness matrix of heterogenous materials in a straightforward manner without relying on ad-hoc assumptions. In particular, the method lays on the concept of Structure Genome (SG), defined as the smallest mathematical building block of the structure, which for the purposes of the present study is equivalent to the Unit Cell.

The macroscopic properties are defined in a global coordinate system, $\boldsymbol{x} = \{x, y, z\}$ (see Figure 1), whereas $\boldsymbol{y} = \{y_1, y_2, y_3\}$ defines the local reference system of the RUC (see Figure 2). These approach is based on the assumption that $y_i = x_i/\delta$, where δ is the scaling parameter, which means that the RUC is much smaller than the whole structure. Subsequently, the information extracted from the RUC analysis is decoupled from the macroscopic problem. Also, it is possible to define an average value of the local fields over the RUC volume:

$$\frac{1}{V}\int_V u_i(\boldsymbol{x}, \boldsymbol{y})\, dV = \bar{u_i}(\boldsymbol{x}) \tag{7}$$

where V is the total volume of the cell. u_i are the local displacements depending on $\boldsymbol{x}$ and $\boldsymbol{y}$ respectively, and $\bar{u_i}$ are the averaged displacements that are only a function of the global coordinates. The periodicity of the RUC is therefore imposed as:

$$\begin{aligned} u_i(x, y, z; \frac{d_1}{2}, y_2, y_3) &= u_i(x + d_1, y, z; -\frac{d_1}{2}, y_2, y_3) \\ u_i(x, y, z; y_1, \frac{d_2}{2}, y_3) &= u_i(x, y + d_2, z; y_1, -\frac{d_2}{2}, y_3) \\ u_i(x, y, z; y_1, y_2, \frac{d_3}{2}) &= u_i(x, y, z + d_3; y_1, y_2, -\frac{d_3}{2}) \end{aligned} \tag{8}$$

The mathematical foundation of MSG is the Variational asymptotic method (VAM), introduced by Berdichevskly [28] for the study of periodic systems. VAM can be used for the analysis of stationary value problems in which certain terms are smaller than others. This method is well-known in the mechanics field, where problems featuring heterogeneities at different scales are very common. For instance, in beam structures, the cross-section is usually smaller than the length, and in shell problems the thickness is often negligible in comparison to the global dimensions. In the case of metamaterials and composite materials, VAM is a powerful mathematical tool due to the several geometrical scales that must be accounted in the analysis.

In MSG, the constitutive information is extracted from the RUC by minimizing the difference in terms of elastic energy between the original heterogeneous cell and the equivalent homogeneous material, which can be written as the following functional:

$$\Pi = \left\langle \frac{1}{2}\, C_{ijkl}\, \varepsilon_{ij}\, \varepsilon_{kl} \right\rangle - \frac{1}{2}\, C^{*}_{ijkl}\, \bar{\varepsilon}_{ij}\, \bar{\varepsilon}_{kl} \tag{9}$$

where $\langle \bullet \rangle$ denotes the volume average $\frac{1}{V}\int_V \bullet\, dV$. The first term of the functional Π is the strain energy of the heterogeneous body, whereas the second term is the strain energy of the homogeneous material. C_{ijkl} is the fourth-order elastic tensor and ε_{ij} is the second-order strain tensor. C^{*}_{ijkl} and $\bar{\varepsilon}_{ij}$ are those of the homogenized body.

The local displacements over the RUC can be written as the sum of the global displacements, $\bar{u}_i$, plus the difference between both, as follows

$$u_i(\boldsymbol{x};\boldsymbol{y}) = \bar{u}_i(\boldsymbol{x}) + \delta\, \chi_i(\boldsymbol{x};\boldsymbol{y}) \tag{10}$$

where χ_i are denoted as fluctuation functions, which are scaled down using δ.

Making use of the derivative of a field at different scales of the type $f(\boldsymbol{x};\boldsymbol{y})$,

$$\frac{\partial f}{\partial x_j} + \frac{1}{\delta}\frac{\partial f}{\partial y_j} \tag{11}$$

and discarding the smaller terms, the strain field results:

$$\varepsilon_{ij}(\boldsymbol{x};\boldsymbol{y}) = \bar{\varepsilon}_{ij}(\boldsymbol{x}) + \chi_{(i,j)}(\boldsymbol{x};\boldsymbol{y}) \tag{12}$$

where

$$\bar{\varepsilon}_{ij}(\boldsymbol{x}) = \frac{1}{2}\Big(\frac{\partial \bar{u}_i(\boldsymbol{x})}{\partial x_j} + \frac{\partial \bar{u}_j(\boldsymbol{x})}{\partial x_i}\Big) \tag{13}$$

and

$$\chi_{(i,j)}(\boldsymbol{x};\boldsymbol{y}) = \frac{1}{2}\Big(\frac{\partial \chi_i(\boldsymbol{x};\boldsymbol{y})}{\partial y_j} + \frac{\partial \chi_j(\boldsymbol{x};\boldsymbol{y})}{\partial y_i}\Big) \tag{14}$$

By means of Eq. (10) and Eq. (12), the fluctuation unknowns, χ_i, that minimize the information loss of the RUC are obtained by minimizing the following functional:

$$\Pi_1 = \frac{1}{2}\Big\langle C_{ijkl}\,(\bar{\varepsilon}_{ij} + \chi_{(i,j)})\,(\bar{\varepsilon}_{kl} + \chi_{(k,l)}) \Big\rangle \tag{15}$$

One can notice that the second term of Eq. (9) does not vary with χ_i, so it can be discarded.

Finally, according to Eq. (7), one can write

$$\bar{u}_i = \langle u_i \rangle \qquad\qquad \bar{\varepsilon}_{ij} = \langle \varepsilon \rangle \tag{16}$$

which lead to the following constrains of the problem:

$$\langle \chi_i \rangle = 0 \qquad\qquad \langle \chi_{(i,j)} \rangle = 0 \tag{17}$$

4.2 CUF 1D models

The Carrera Unified Formulation allows to develop refined models in which the theory order and approximation type become free parameters, introduced as input of the problem. The CUF describes the kinematic field in a unified manner which is then used to describe the governing equations in a hierarchical and compact way.

Consider a local coordinate system for the micro-scale problem as the one shown in Figure 2. The beam

axis, y_3, is chosen to be the pore direction, whose total length is equal to L, whereas the heterogeneities over the section lie on the y_1y_2-plane, in correspondence with the cross-section of the beam, Ω. Classical beam models are not a suitable choice to solve the RUC problem. CUF sets a framework in beam modeling in which the kinematic assumptions are axiomatically introduced in the structural analysis, in such a way that higher-order effects can be represented by the theory of structure. For the present purposes, the fluctuation unknowns can be expanded over the cross-section by means of arbitrary functions of the y_1 and y_2 coordinates, as follows

$$\boldsymbol{\chi}(\boldsymbol{x}; y_1, y_2, y_3) = F_\tau(y_1, y_2)\, \boldsymbol{\chi}_\tau(\boldsymbol{x}; y_3) \quad \tau = 1, 2, ..., M \tag{18}$$

where $\boldsymbol{\chi}$ is the vector of the fluctuations, F_τ are the expanding functions and $\boldsymbol{\chi}_\tau$ is the vector of the generalized fluctuations of the beam along the fibre-direction. The repeated subscript τ denotes summation and M is the total number of expansion terms assumed for the kinematic field. The choice of F_τ defines the beam theory of the analysis.

At the same time, the pore direction is discretized by means of standard beam elements. Lagrange-class shape functions are used to interpolate the fluctuation unknowns, $\boldsymbol{\chi}_\tau$, along y_1

$$\boldsymbol{\chi}_\tau(\boldsymbol{x}; y_3) = N_i(y_3)\, \boldsymbol{\chi}_{\tau i}(\boldsymbol{x}) \quad i = 1, 2, ..., n \tag{19}$$

where $\boldsymbol{\chi}_{\tau i}(\boldsymbol{x})$ is the nodal unknown vector and n is the total number of beam nodes.

In order to capture all the information of the RUC, the beam theory must be able to represent the exact geometry of the body and enable the application of the periodic boundary conditions over the edges. For this, the Hierarchical Legendre Expansions (HLE) is chosen to expand the unknowns over the cross-sectional coordinates.

4.2.1 Hierarchical Legendre Expansion

The choice of $F_\tau(x, y)$ determines the class of beam theory adopted. The method investigated employs a HLE model, *i.e.* a set of hierarchical Legendre-like polynomials as $F_\tau(x, y)$ generic functions of the cross-section domains [22]. In the code at hand, the polynomials used in HLE beam theory can be chosen from the first to eighth order. This hierarchical set is used in quadrilateral nodal, edge and internal expansions.
The hierarchy of this model implies that the set of functions of a given order also contains the polynomials of lower degrees. For example, the sixth-order HLE model contains $M = 30$ terms in the expansion. As a result, the accuracy of the approximation can be enhanced by the polynomial order of the theory, which allows to use coarse discretization at the cross-sectional level.

Usually, conventional finite elements use isoparametric formulations to map the geometry of the structure, so that the shape of the physical boundaries of the domain is described by the same functions that are used to interpolate the unknown variables. When elevated expansion orders of HLE are used, the domain discretization of the cross-section surface can be very coarse. Therefore, using isoparametric formulation would lead to very inaccurate geometry. For this reason, the proposed method makes use of a non-isoparametric mapping technique based on the blending function method, introduced by Gordon *et al.* [29]. The blending function method allows a description of the geometry independent of the expansion functions $F_\tau(x, y)$. Curved boundaries (as the cylindrical holes described in the previous section) of large domains are represented accurately even with coarse cross-section discretization. Thus, this method allows significant reduction of the error related to the geometrical approximation, and a reduction on the computational efforts. For more details about HLE beam elements applied to microstructures, the reader can refer to [30].

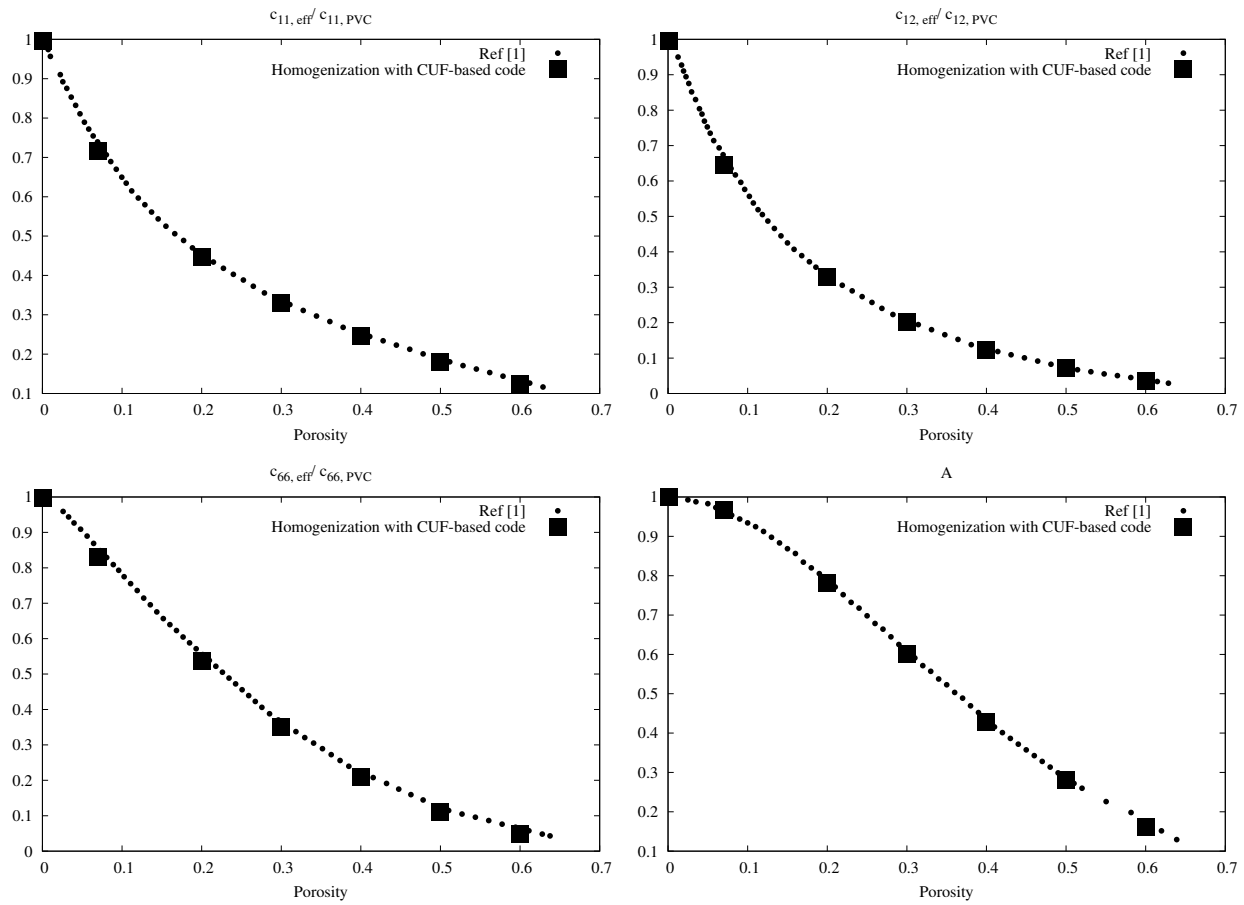

Figure 3: Porosity variation of the homogenized coefficients of the stiffness matrix $c_{11,\text{eff}}/c_{11,\text{PVC}}$, $c_{12,\text{eff}}/c_{12,\text{PVC}}$, $c_{66,\text{eff}}/c_{66,\text{PVC}}$ and porosity variation of the anisotropic coefficient A.

5 Comparison of the homogenisation methods for 2D unit cells

For the sake of comparison, the unit cell (UC) investigated to assess the quality of the homogenization process with this new method is chosen as in Langlet et al. [19] as shown in Figure 1b, i.e. a matrix surrounding a cylindrical void. As in [19], the material is PVC with $E = 3.78 \times 10^9$ Pa, $\nu = 0.4$ and $\rho = 1430$ kg.m^{-3}. In [19], it is assumed that the unit-cell is infinite in the z-direction.
The code is able to accommodate this unit cell geometry as it is similar to a fiber-reinforced composite material, with the material properties of the fiber set up as zero. Porosity of the material is defined as $P = \frac{\pi r^2}{d^2}$ where r is the radius of the void cylinder and d is the side of the unit cell, and can vary from 0 to $\frac{\pi}{4}$.

Figure 3 presents the porosity variation of the normalized homogenized stiffness coefficients $c_{11,\text{eff}}/c_{11,\text{PVC}}$, $c_{12,\text{eff}}/c_{12,\text{PVC}}$, $c_{66,\text{eff}}/c_{66,\text{PVC}}$ where $c_{11,\text{PVC}}$, $c_{12,\text{PVC}}$ and $c_{66,\text{PVC}}$ are the PVC stiffness constants. The anisotropic coefficient A is defined as $A = \frac{2c_{66,\text{eff}}}{c_{11,\text{eff}} - c_{12,\text{eff}}}$. Results obtained with the CUF-MSG-based method are in accordance with Langlet et al. [19], thus validating the method for 2D Unit-cells.

6 Effective properties of a 3D perforated plate

It is now assumed that the plate is not infinite in the z-direction anymore. The Unit-Cell remains the same but the plate has a given thickness as in Figure 1a.

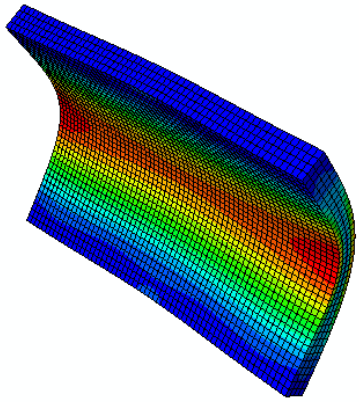

Figure 4: Example of free vibration modal analysis for the 600-holes homogenized plate on ABAQUS with 4 elements layers in the thickness. Modal frequency $f = 646.7$ Hz.

In the CUF-MSG based method, the periodicity of the array of void-cylinders has to be respected and the size of the unit cell has to be small compared to the dimension of the plates. If so, at a given porosity the results should stay the same, no matter the shape of the UC and its actual size compared to the plate. Inputs of the code are only geometry of the unit cell (cylinder or inclusion), material engineering constants, porosity and highest polynomial order of the Hierarchical Lagrange Expansion model. Outputs are the stiffness matrix of the orthotropic equivalent material, and the engineering constants.

As mentioned previously, the method was originally designed and tested for composites where the scale of the UC is much smaller than the dimensions of the plate and the pores or the fibers are in the longitudinal direction. Our aim is to verify if the homogenization process is also efficient for a plate such as Figure 1a, where the pores are visible, open, and oriented in the normal direction of the plate. Langlet et al. [19] conducted experiments on one full plate of PVC and two perforated plates of PVC with 300 holes ($P = 0.192$) and 600 holes ($P = 0.385$).

Experimental resonance frequencies are measured using an accelerometer applied on the plates excited by a harmonic sound. The plate are 20 mm thick (z-direction), 309 mm long (x-direction) and 206 mm wide (y-direction). The hole diameter is 7 mm.

In Langlet et al. [19], a tridimensional unit cell is meshed containing one pore of arbitrary thickness along the z-direction, therefore there is only one layer of elements in the thickness. The finite elements method explained in Section 1 yields quasi-transverse and quasi-longitudinal velocities, and the Christoffel's equations give the homogeneous material stiffness tensor. Using these effective properties, the perforated plates are meshed as homogeneous and anisotropic plates so that the meshing of 300 or 600 holes is avoided. A modal analysis is then conducted providing the resonance frequencies of the plates in free-boundary conditions. These results are compared to the experimental resonance frequencies.

In order to obtain the resonance frequencies corresponding to the homogenized materials obtained with the CUF-MSG based method, two methods are used. On the one hand, the commercial software ABAQUS is used to analyze a tridimensional model of the plate with the homogenized mechanical properties and the efficient density calculated as in Eq. 5. The mesh used holds approximately 10000

3D quadratic elements, with four layers of elements within the thickness of the plate. The seeds in the x and y directions are set so that the elements are approximately cubic, as shown in Figure 4. 62 and 41 elements are inserted in respectively the x-direction and the y-direction.
On the other hand, a finite element code also based on the Carrera Unified Formulation, called MUL2, is used to calculate the resonance frequencies of the homogenized plate. Following, a brief description of this model.

7 CUF 2D models

In the framework of CUF 2D models, the displacement field is written by means of approximating functions in the thickness direction as follows:

$$\boldsymbol{u}(x,y,z) = F_\tau(z)\boldsymbol{u}_\tau(x,y) \qquad \tau = 0,1,...,N \tag{20}$$

F_τ are the so-called thickness functions depending only on z. $\boldsymbol{u}_\tau$ are the unknown variables depending on the coordinates x and y. τ is a sum index and N is the order of expansion in the thickness direction assumed for the displacements.

In particular, the displacement is defined as:

$$\boldsymbol{u} = F_t\,\boldsymbol{u}_t + F_b\,\boldsymbol{u}_b + F_r\,\boldsymbol{u}_r = F_\tau\,\boldsymbol{u}_\tau, \qquad \tau = t,b,r\ , \quad r = 2,...,N. \tag{21}$$

where F_τ are linear combinations of Legendre polynomials:

$$F_t = \frac{P_0 + P_1}{2}, \quad F_b = \frac{P_0 - P_1}{2}, \quad F_r = P_r - P_{r-2}. \tag{22}$$

$P_j = P_j(\zeta)$ is the Legendre polynomial of j-order defined in the ζ-domain: $-1 \leq \zeta \leq 1$. The top (t) and bottom (b) values of the displacements are used as unknown variables.
If FEM approximation is introduced for the general displacements in the plane of the plate, one has:

$$\boldsymbol{u}_\tau(x,y) = N_i(\xi,\eta)\boldsymbol{q}_{\tau i}, i = 4,8,9 \tag{23}$$

where N_i are the Lagrangian shape functions, (ξ,η) are the non-dimensional local coordinates in the plane of the plate, $\boldsymbol{q}_{\tau i}^T = \{q_{x_{\tau i}}, q_{y_{\tau i}}, q_{z_{\tau i}}\}$ are the nodal displacements.
A thorough description of the CUF method for general finite elements formulations and plate theories introduced in the past years can be found in the book of Carrera et al. [20].

7.1 Free-vibration analysis

This section presents the derivation of the governing finite element stiffness matrix and mass matrix based on the Principle of Virtual Displacements (PVD) in the case of free-vibration analysis of plates.

The PVD can be written as follows:

$$\int_\Omega \int_A \left\{ \delta{\boldsymbol{\epsilon}_p}^T \boldsymbol{\sigma}_p + \delta{\boldsymbol{\epsilon}_n}^T \boldsymbol{\sigma}_n \right\} d\Omega dz = \int_\Omega \int_A \rho\, \delta\boldsymbol{u}\, \ddot{\boldsymbol{u}}\, d\Omega dz \tag{24}$$

where Ω and A are the integration domains on the midsurface and in the thickness direction, respectively. The member on the left hand side of the equation represents the variation of the internal work, while the member on the right hand side of the equation represents the kinetic energy due to the inertia. ρ stands for the density of the material, and $\ddot{\boldsymbol{u}}$ is the acceleration vector.

Substituting the constitutive equations (3), the geometrical relations (1) and applying the Unified Formulation (20) and the FEM approximation (23), one obtains the following governing equations:

$$\delta \boldsymbol{q}_{\tau_i} : \quad \boldsymbol{K}^{\tau sij} \boldsymbol{q}_{s_j} = \boldsymbol{M}^{\tau sij} \ddot{\boldsymbol{q}}_{s_j} \tag{25}$$

where the indexes s and j are analogous to τ and i, respectively, and they are introduced for the approximation of displacements virtual variation $\delta \boldsymbol{u}$.
$\boldsymbol{K}^{\tau sij}$ and $\boldsymbol{M}^{\tau sij}$ are 3×3 matrix, called fundamental nuclei, and their explicit expressions are provided in the book [20]. These are the basic elements from which the stiffness matrix and mass matrix of the whole structure are computed. The final form of the free-vibration problem can be written as it follows:

$$-\boldsymbol{M}\ddot{\boldsymbol{q}} + \boldsymbol{K}\boldsymbol{q} = 0 \tag{26}$$

where $\boldsymbol{q}$ is the vector of the nodal displacements. Introducing harmonic solutions, it is possible to compute the natural frequencies ω_l, by solving an eigenvalues problem:

$$-(\omega_l^2 \boldsymbol{M} + \boldsymbol{K})\boldsymbol{q}_l = 0 \tag{27}$$

where $\boldsymbol{q}_l$ is the l-th eigenvector.

8 Results

Engineering constants of the homogeneous equivalent plates of perforated PVC are found in Table 1. As mentioned before, they are derived from the CUF-MSG-based homogenization method explained in Subsection 2.2. Full PVC ($E = 3.78 \times 10^9$ Pa, $\nu = 0.4$ and $\rho = 1430$ kg.m^{-3}) is used as the matrix and the volume fraction is chosen as in [19] ($P = 0.192$ and $P = 0.385$ for resp. 300 and 600 holes), which yields the density of the homogenized plate thanks to Eq. (5).
The subscripts 1, 2, 3 refer to x, y and z respectively where (x, y, z) is set as in Figure 1a with z in the direction of the holes and normal direction of the plate.

	300 Holes	600 Holes
Density (kg.m^{-3})	1155.44	879.45
E_1 (GPa)	2.442544217	1.624513970
E_2 (GPa)	2.442544219	1.624513972
E_3 (GPa)	3.053097271	2.322408590
G_{12} (GPa)	0.7455780024	0.3071786601
G_{13} (GPa)	0.9143532202	0.5951974724
G_{23} (GPa)	0.9143532207	0.5951974731
ν_{12}	0.3042371111	0.1954291087
ν_{13}	0.4000000000	0.4000000000
ν_{23}	0.4000000000	0.4000000000

Table 1: Engineering constants of the homogenized materials obtained by the CUF-MSG based code.

8.1 Modal analysis of equivalent homogeneous plates compared to experimental results

The natural frequencies are shown in Table 5, Table 6 and Table 7.
A convergence study is performed in Table 2, Table 3 and Table 4 for the MUL2 Finite Element code

6×6 - 1 L2 (Hz)	12×12 - 1 L2 (Hz)	46×30 1 L2 (Hz)	46×30 2 L2 (Hz)	ABAQUS (Hz)
307.83	306.27	305.83	304.82	304.73
346.72	346.40	346.37	346.08	346.06
709.63	704.78	703.31	700.12	699.84
817.08	816.06	815.88	814.33	814.21
892.24	887.98	887.32	884.40	884.16
1085.78	1079.88	1078.97	1074.83	1074.5
1307.45	1294.14	1291.27	1283.67	1283
1481.41	1470.76	1467.95	1458.29	1457.5
1914.63	1871.91	1868.81	1857.89	1857

Table 2: Full PVC - Convergence Study and comparison with 62x41x4 ABAQUS Mesh

.

6×6 - 1 L2 (Hz)	12×12 - 1 L2 (Hz)	46×30 1 L2 (Hz)	46×30 2 L2 (Hz)	ABAQUS (Hz)
256.74	254.78	254.30	253.54	253.47
309.43	309.34	309.26	309.03	309.01
601.02	596.26	594.82	592.50	592.29
708.78	709.23	708.99	707.82	707.74
796.05	792.10	791.38	789.10	788.91
920.74	917.80	916.94	914.00	913.78
1127.34	1116.05	1113.38	1107.79	1107.3
1258.93	1249.60	1246.84	1239.78	1239.2
1662.67	1632.66	1629.84	1621.43	1620.8

Table 3: PVC 300 Holes - Convergence Study and comparison with 62x41x4 ABAQUS Mesh

.

6×6 - 1 L2 (Hz)	12×12 - 1 L2 (Hz)	46×30 1 L2 (Hz)	46×30 2 L2 (Hz)	ABAQUS (Hz)
191.61	190.58	191.61	189.66	189.6
288.86	288.63	288.86	288.39	288.38
480.69	477.95	480.69	475.32	475.17
648.36	647.82	648.36	646.72	646.65
722.87	720.48	722.87	718.13	717.97
810.26	806.11	810.26	803.44	803.27
961.25	953.16	961.25	947.31	946.97
1030.85	1024.73	1030.85	1018.04	1017.6
1416.17	1414.87	1416.17	1414.76	1414.8

Table 4: PVC 600 Holes - Convergence Study and comparison with 62x41x4 ABAQUS Mesh

.

(9-nodes standard Lagrangian elements are used) with four different meshes and the three types of plates : 6×6, 12×12 and 46×30 in the (x, y) dimension with a single layer and quadratic expansion through the thickness. In this case the solution is indicated as 1 L2. The final mesh is 46×30 in the (x, y) with two layers and quadratic expansion through the thickness of each layer, also shown in Figure 5. In this case, the solution is 2 L2.

ABAQUS (Hz)	MUL2 46 × 30 2 L2 (Hz)	FEM[19] (Hz)	Exp.[19] (Hz)	Rel. Err. [19] %	Rel. Err. MUL2 %
304.73	304.82	305.60	307	-0.46	-0.71
346.06	346.08	346.30	355	-2.45	-2.51
699.84	700.12	702.80	701	0.26	-0.13
814.21	814.33	815.00	815	0.00	-0.08
884.16	884.40	886.00	902	-1.77	-1.95
1074.5	1074.83	1078.00	1075	0.28	-0.02
1283	1283.67	1290.40	1257	2.66	2.12
1457.5	1458.29	1463.70	1462	0.12	-0.25
1857	1857.89	1873.10	1867	0.33	-0.49

Table 5: Full PVC - Modal frequencies and Relative Errors of FEM [19], ABAQUS and MUL2 code with refined mesh compared to experimental results of [19]

.

ABAQUS (Hz)	MUL2 46 × 30 2 L2 (Hz)	FEM[19] (Hz)	Exp.[19] (Hz)	Rel. Err. [19] %	Rel. Err. MUL2 %
253.47	253.54	282.00	272	3.68	-6.79
309.01	309.03	288.60	289	-0.14	6.93
592.29	592.50	634.10	621	2.11	-4.59
707.74	707.82	680.20	681	-0.12	3.94
788.91	789.10	755.60	748	1.02	5.49
913.78	914.00	919.40	901	2.04	1.44
1107.3	1107.79	1134.80	1116	1.68	-0.74
1239.2	1239.78	1302.90	1271	2.51	-2.46
1620.8	1621.43	1577.30	1548	1.89	4.74

Table 6: PVC with 300 Holes - Modal frequencies and Relative Errors of FEM [19], ABAQUS and MUL2 code compared to experimental results of [19]

.

ABAQUS (Hz)	MUL2 46 × 30 2 L2 (Hz)	FEM[19] (Hz)	Exp.[19] (Hz)	Rel. Err. [19] %	Rel. Err. MUL2 %
189.6	189.66	192.20	180	6.78	5.37
288.38	288.39	289.20	273	5.93	5.64
475.17	475.32	480.50	459	4.68	3.55
646.65	646.72	648.20	626	3.55	3.31
717.97	718.13	721.90	690	4.62	4.08
803.27	803.44	807.50	772	4.60	4.07
946.97	947.31	956.10	925	3.36	2.41
1017.6	1018.04	1027.30	1005	2.22	1.30
1414.8	1414.76	1424.30	1442	-1.23	-1.89

Table 7: PVC with 600 Holes - Modal frequencies and Relative Errors of FEM [19], ABAQUS and MUL2 code compared to experimental results of [19]

.

For the full plate, 300 holes and 600 holes, all results seem to converge towards the results obtained with ABAQUS. They are close but do not converge toward the experimental results for 300 holes. This

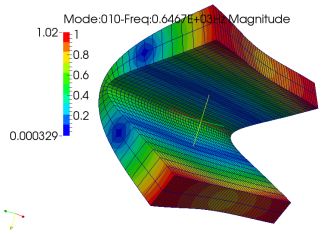

Figure 5: Example of free vibration modal analysis for the 600-holes homogenized plate with final mesh 46x30 and 2 quadratic beam elements in the thickness. Visualisation on ParaView of the MUL2 FEM solver results for Modal frequency $f = 646.7$ Hz.

can be expected as ABAQUS and the MUL2 code consider the same problem with the same geometry, same approximations and same homogenized engineering constants.

As expected, the results of the CUF-MSG based method are closer to experiments as the number of holes increases. The more dense is the grid of holes, the more are respected the periodicity assumptions in which the CUF-MSG method is based. For 600 holes the error in the solutions is similar to that of the literature.

In all cases, computation time is shorter than with ABAQUS and results are still within 10% Relative Error with regards to experimental results.

9 Conclusion

The results show that the homogenization method based on CUF and MSG method is efficient to predict the stiffness matrix and the modal frequencies of the perforated plate while avoiding 2D assumptions and meshing the holes. Relative errors to the experiments are always below 10% and give the same accuracy as a full FEM homogenization method like [19] with few calculations.

The importance of the periodicity assumption is highlighted with these results. The more dense is the grid of unit cells, the closer is the homogenization to experiments on plates with holes.

It remains to be verified if this method, which is without losses and doesn't take into account the air inside the holes, is sufficient to properly predict the acoustic properties of the material, such as the Sound Transmission Loss. Future investigation will focus on testing these homogenized materials acoustically with commercial software Actran.

References

[1] R. Liu, C. Ji, Z. Zhao, and T. Zhou. Metamaterials: Reshape and rethink. *Engineering*, 1(2):179–184, 2015.

[2] C. Caloz. Perspectives on em metamaterials. *Materials Today*, 12(3):12–20, 2009.

[3] P. Alitalo and S. Tretyakov. Electromagnetic cloaking with metamaterials. *Materials Today*, 12(3):22–29, 2009.

[4] R. Grimberg. Electromagnetic metamaterials. *Materials Science and Engineering: B*, 178(19):1285–1295, 2013.

[5] K. Fan and W.J. Padilla. Dynamic electromagnetic metamaterials. *Materials Today*, 18(1):39–50, 2015.

[6] A.A. Zadpoor. Mechanical meta-materials. *Materials Horizon*, 3(5):371–381, 2016.

[7] C. Coulais, D. Sounas, and A. Alù. Static non-reciprocity in mechanical metamaterials. *Nature*, 542:461–464, 2017.

[8] K. Bertoldi, V. Vitelli, J. Christensen, and M. van Hecke. Flexible mechanical metamaterials. *Nature Reviews Materials*, 2(17066), 2017.

[9] Z. Yang, J. Mei, M. Yang, N.H. Chan, and P. Sheng. Membrane-type acoustic metamaterial with negative dynamic mass. *Physical Review Letters*, 101:204301, 2008.

[10] G. Ma and P. Sheng. Acoustic metamaterials: From local resonances to broad horizons. *Science Advances*, 2(2):e1501595, 2016.

[11] D. Lee, D.M. Nguyen, and J. Rho. Acoustic wave science realized by metamaterials. *Nano Convergence*, 4:3:DOI 10.1186/s40580–017–0097–y, 2017.

[12] D. Gao, X. Zeng, X. Liu, and K. Han. Resonant modes of one-dimensional metamaterial containing helmholtz resonators with point defect. *Journal of Modern Physics*, 8:1737–1747, 2017.

[13] C. Elachi. Waves in active and passive periodic structures: A review. *Proceedings of the IEEE*, 64(12):1666–1698, 1977.

[14] A. Singh, D.J. Pines, and A. Baz. Active/passive reduction of vibration of periodic one-dimensional structures using piezoelectric actuators. *Smart Materials and Structures*, 13(4):698, 2004.

[15] L. Zheng, Y. Li, and A. Baz. Attenuation of wave propagation in a novel periodic structure. *Journal of Central South University of Technology*, 18(2):438–443, 2011.

[16] G. Mathur. Novel sound absorptive materials based on acoustic metamaterial principles. In *23rd International Congress on Sound & Vibration ICSV23*.

[17] A.-C. Hladky-Hennion and J.-N. Decarpigny. Analysis of the scattering of a plane acoustic wave by a doubly periodic structure using the finite element method: Application to alberich anechoic coatings. *The Journal of the Acoustical Society of America*, 90(6):3356–3367, 1991.

[18] C. Conca and M. Vanninathan. Homogenization of periodic structures via bloch decomposition. *SIAM Journal on Applied Mathematics*, 57(6):1639–1659, 1997.

[19] P. Langlet, A.-C. Hladky-Hennion, and J.-N. Decarpigny. Analysis of the propagation of plane acoustic waves in passive periodic materials using the finite element method. *The Journal of the Acoustical Society of America*, 98(5):2792–2800, 1995.

[20] E. Carrera, M. Cinefra, M. Petrolo, and E. Zappino. *Finite element analysis of structures through unified formulation*. John Wiley & Sons, 2014.

[21] W. Yu. A unified theory for constitutive modeling of composites. *Journal of Mechanics of Materials and Structures*, 11(4):379–411, 2016.

[22] A.G. de Miguel, A. Pagani, W. Yu, and E. Carrera. Micromechanics of periodically heterogeneous materials using higher-order beam theories and the mechanics of structure genome. *Composite Structures*, 180:484–496, 2017.

[23] M. Cinefra. Free-vibration analysis of laminated shells via refined mitc9 elements. *Mechanics of Advanced Materials and Structures*, 23(9):937–947, 2016.

[24] E. Reissner. The effect of transverse shear deformation on the bending of elastic plates. 1945.

[25] R.D. Mindlin. Influence of rotary inertia and shear on flexural motions of isotropic elastic plates. 1951.

[26] A.S.L. Chan. Variational methods in elasticity and plasticity. k. washizu. pergamon, oxford, 1968. 350 pp. illustrated. 120s. *The Aeronautical Journal (1968)*, 72(694):889–889, 1968.

[27] O. Doutres, N. Atalla, and H. Osman. Transfer matrix modeling and experimental validation of cellular porous material with resonant inclusions. *The Journal of the Acoustical Society of America*, 137(6):3502–3513, 2015.

[28] V.L. Berdichevskii. On averaging of periodic systems. *Journal of Applied Mathematics and Mechanics*, 41(6):1010 – 1023, 1977.

[29] W.J. Gordon and C.A. Hall. Transfinite element methods: blending-function interpolation over arbitrary curved element domains. *Numerische Mathematik*, 21(2):109–129, 1973.

[30] A. Pagani, A.G. de Miguel, and E. Carrera. Component-wise analysis of laminated structures by hierarchical refined models with mapping features and enhanced accuracy at layer to fiber-matrix scales. *Mechanics of Advanced Materials and Structures*, 2017. In Press.